Letter

Density matrix renormalization group boosted by Gutzwiller projected wave functions

Hui-Ke Jin [1], Hong-Hao Tu [2,*] and Yi Zhou [1,3,4,†]

[1] *Beijing National Laboratory for Condensed Matter Physics & Institute of Physics, Chinese Academy of Sciences, Beijing 100190, China*

[2] *Institut für Theoretische Physik, Technische Universität Dresden, 01062 Dresden, Germany*

[3] *Songshan Lake Materials Laboratory, Dongguan, Guangdong 523808, China*

[4] *Kavli Institute for Theoretical Sciences & CAS Center for Excellence in Topological Quantum Computation, University of Chinese Academy of Sciences, Beijing 100190, China*

(Received 10 September 2020; accepted 6 July 2021; published 15 July 2021)

We propose to boost the performance of the density matrix renormalization group (DMRG) in two dimensions by using Gutzwiller projected states as the initialization *Ansatz*. When the Gutzwiller projected state is properly chosen, the notorious "local minimum" issue in DMRG can be circumvented and the precision of DMRG can be improved by orders of magnitude without extra computational cost. Moreover, this method allows one to quantify the closeness of the initial Gutzwiller projected state and the final converged state after DMRG sweeps, thereby shedding light on whether the Gutzwiller *Ansatz* captures the essential entanglement features of the actual ground state for a given Hamiltonian. Kitaev honeycomb model has been exploited to demonstrate and benchmark this method.

DOI: 10.1103/PhysRevB.104.L020409

Since its invention [1,2], the density matrix renormalization group (DMRG) has been recognized as the most powerful computational method for studying strongly correlated quantum systems in one dimension [3–5]. Soon after that, it was realized that DMRG can be formulated as a variational method operating within the family of matrix product states (MPSs) [6,7]. This discovery led to a deeper and coherent understanding of the inner structure of the DMRG method, as well as its potential and limitations [8,9]. For instance, it became clear that DMRG is only moderately successful when applied to two-dimensional (2D) quantum systems [10].

The sharply distinct performance of DMRG in one and two dimensions originates from the different entanglement scaling with respect to spatial dimensionality, dictated by the so-called area law [11–13]. For 2D systems, the common practice of DMRG is to consider lattices with cylindrical boundary conditions and gradually increase the circumference of the cylinder [10]. However, the convergence of DMRG is not guaranteed due to the presence of local minima in the energy landscape. As a result, the efficiency and accuracy of DMRG highly depend on how the initial states are chosen. It is expected that the performance of DMRG can be improved by using some initial states that capture the essential physics. Actually, Gutzwiller projected wave functions have long been used as variational *Ansatzë* for strongly correlated systems [14–17].

This raises a very natural question: Can one utilize Gutzwiller projected wave functions to improve the performance of DMRG? Very recently, it was proposed by us [18] and co-workers [19] that a Gutzwiller projected state can be efficiently converted to an MPS by using the so-called matrix product operator–matrix product state (MPO-MPS) method. This completes the building block of initializing DMRG with Gutzwiller projected states. The accuracy of the MPO-MPS method has already been carefully examined for various one-dimensional systems [18,19]. Along this line, the present Letter focuses on (1) sorting out the subtleties of the MPO-MPS method for 2D systems with cylindrical boundary conditions and (2) analyzing the performance of DMRG initialized with Gutzwiller projected states.

The Kitaev honeycomb model [20], being a rare exactly solvable example in two dimensions, is used for illustrating our method. Our extensive analysis shows that the MPO-MPS method, with several subtleties taken into account, converts Gutzwiller projected states into MPSs with satisfactory precision and the performance of DMRG is dramatically improved when initialized with these MPSs. We also address a controversial issue: With a magnetic field in the [111] direction, the Kitaev honeycomb model (with antiferromagnetic interactions) was claimed to support a disordered state at intermediate field strength [21–23]. We use our method to analyze several candidate wave functions [24,25] and found that although some of them describe actual ground states well in both small and large field limits, all of them seem to fail for intermediate field strengths, thus calling for further investigations on the nature of the field-induced disordered state.

Method. Throughout this Letter, we consider spin-1/2 lattice systems and Gutzwiller projected states with singly occupied fermionic partons at each site [see Fig. 1(a)], whereas generalizations to other systems are straightforward. Our method consists of three main steps:

(1) Construct the Gutzwiller projected state as $|\Psi_G\rangle = P_G|\Psi_0\rangle$, where $|\Psi_0\rangle$ is the ground (or excited) state of a

*hong-hao.tu@tu-dresden.de

†yizhou@iphy.ac.cn

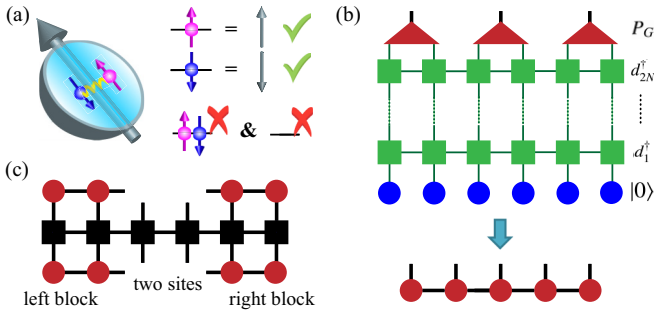

FIG. 1. (a) Sketch of parton construction for a quantum spin-1/2 system, where Gutzwiller projection keeps two single-occupied states and removes other components locally. (b) Convert a Gutzwiller projected wave function into an MPS by the MPO-MPS method. (c) The MPS prepared in (b) serves as an initial state for two-site DMRG.

quadratic Hamiltonian for fermionic partons and P_G is the Gutzwiller projector imposing single-occupancy constraint.

(2) Convert $|\Psi_G\rangle$ into an MPS by using the MPO-MPS method [18,19] as illustrated in Fig. 1(b), and keep the bond dimension of the resulting MPS up to $\tilde{D}$.

(3) Use the two-site DMRG algorithm [5] to optimize the MPS obtained in step (2) with respect to the target Hamiltonian [see Fig. 1(c)], where the bond dimension of MPS is gradually increased from $\tilde{D}$ to D.

Model. To demonstrate the performance of our method, we first consider the Kitaev honeycomb model [20] in the presence of three-spin interactions,

$$\mathcal{H}_3 = \sum_a \sum_{\langle jk\rangle\in a} J_a \sigma_j^a \sigma_k^a + J_3 \sum_{\langle jkl\rangle\in\triangle} \sigma_j^x \sigma_k^y \sigma_l^z, \tag{1}$$

where σ_j^a $(a = x, y, z)$ are Pauli matrices, $\langle jk\rangle \in a$ denotes a nearest-neighbor (NN) bond of type a [see Fig. 2(a)], and $\langle jkl\rangle \in \triangle$ refers to three sites around two types of triangles as indicated in Fig. 2(a), as well as their translations to the whole lattice.

We use Kitaev's Majorana representation, $\sigma_j^a = ic_j^a c_j^0$, where c^a (c^0) are so-called gauge (itinerant) Majorana fermions. This representation enlarges the Hilbert space and a local constraint $D_j \equiv c_j^x c_j^y c_j^z c_j^0 = 1$ has to be imposed to restore the physical Hilbert space. Under this representation, $\mathcal{H}_3$ becomes

$$H_{\text{eff}} = -i \sum_a \sum_{\langle jk\rangle\in a} J_a u_{jk} c_j^0 c_k^0 - iJ_3 \sum_{\langle jkl\rangle\in\triangle} u_{jk} u_{kl} c_j^0 c_l^0, \tag{2}$$

where $u_{jk} \equiv ic_j^a c_k^a$ lives on an a-type bond. Since $[H_{\text{eff}}, u_{jk}] = [u_{jk}, u_{lm}] = 0$ for all different bonds, u_{jk} are static $\mathbb{Z}_2$ gauge fields taking their eigenvalues ± 1. When the gauge field configuration (denoted by $\{u\}$) is fixed, H_{eff} becomes a quadratic Hamiltonian of itinerant Majorana fermions, whose eigenstates can be written as $|\phi(\{u\})\rangle$. Together with the state of gauge Majorana fermions denoted by $|\{u\}\rangle$, the eigenstates of H_{eff} read

$$|\Psi_0\rangle = |\{u\}\rangle \otimes |\phi(\{u\})\rangle. \tag{3}$$

These states become (physical) eigenstates of the spin Hamiltonian $\mathcal{H}_3$ after performing the Gutzwiller projection, i.e.,

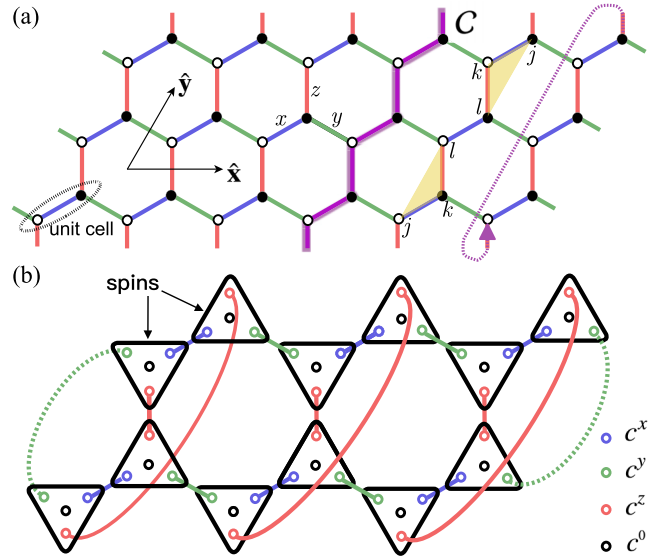

FIG. 2. (a) Kitaev honeycomb model on a cylinder geometry with two basis vectors $\hat{\mathbf{x}}$ and $\hat{\mathbf{y}}$, in which the x boundary is open while the y boundary is periodic. Black dots and white circles stand for A and B sublattices. x, y, and z denote three types of bonds. The three-spin interactions in Eq. (1) are defined on two types of triangles with vertices j, k, and l. The purple zigzag line indicates a closed loop C along which the Wilson loop operator W_y is defined [see Eq. (4)]. (b) Graphic representation of Kitaev's four-Majorana decomposition of spins. Solid bonds stand for the $\mathbb{Z}_2$ gauge field u_{jk}. Dashed bonds emanating from the x boundary indicate how to fix the unpaired boundary modes.

$|\Psi_G\rangle = P_G|\Psi_0\rangle$ with $P_G \equiv \prod_j (1 + D_j)/2$. Here, the projection onto the singly occupied subspace can be revealed by combining Majoranas into complex fermions via $f_{j,\uparrow} = (c_j^x - ic_j^y)/2$ and $f_{j,\downarrow} = (c_j^z - ic_j^0)/2$, so that the local constraint becomes $\sum_{\sigma=\uparrow,\downarrow} f_{j,\sigma}^\dagger f_{j,\sigma} = 1$. Accordingly, the ground state is achieved by determining the gauge field configuration $\{u\}$ in Eq. (2) under which the resulting quadratic Hamiltonian of itinerant Majoranas has the lowest energy.

MPO-MPS process. In correspondence with the common practice in DMRG, we adopt cylindrical boundary conditions, where the honeycomb lattice is embedded on a finite cylinder with L_x (L_y) unit cells along the open (periodic) direction and a total number of $N = 2L_xL_y$ sites. The Hamiltonian $\mathcal{H}_3$ now commutes with Wilson loop operators wrapping around the cylinder, e.g., $W_y = -\prod_{j\in C} \sigma_j^y$, with C being a closed loop shown in Fig. 2(a). The eigenvalue of W_y is just the product of the static $\mathbb{Z}_2$ gauge fields along the loop,

$$W_y|\Psi_G\rangle = \Phi_y|\Psi_G\rangle, \tag{4}$$

where $\Phi_y = \prod_{\langle jk\rangle\in C} u_{jk} = \pm 1$.

The ground-state gauge configuration $\{u\}$ in the $\Phi_y = 1$ sector can be chosen as $u_{jk} = 1$ for all bonds, while for the $\Phi_y = -1$ sector it is achieved by setting $u_{jk} = -1$ for a row of z bonds and $u_{jk} = 1$ elsewhere [20]. Here, we use the convention that j (k) belongs to the A (B) sublattice [see Fig. 2(a)]. However, it is worth emphasizing that, for each sector, there are still unpaired c^y gauge Majorana fermions at the leftmost and rightmost boundaries [see Fig. 2(a)], which

do not enter into the Hamiltonian H_{eff} and thus lead to extra degeneracies.

The MPO-MPS method seeks to minimize the entanglement growth, so we pair up these boundary gauge Majorana fermions [see Fig. 2(b)] into complex fermions $f_{\langle\langle jl\rangle\rangle} \equiv (c_j^y - ic_l^y)/2$ and require that these boundary modes are unoccupied in the unprojected state $|\Psi_0\rangle$, i.e., $f_{\langle\langle jl\rangle\rangle}|\Psi_0\rangle = 0$ for all such boundary modes. Apparently, this manipulation is of great help in suppressing entanglement [26].

With these prescriptions, we are ready to convert the Gutzwiller projected state $|\Psi_G\rangle = P_G|\Psi_0\rangle$ into an MPS by noticing that $|\Psi_0\rangle = \prod_{m=1}^{2N} d_m^\dagger|0\rangle$, where $|0\rangle$ is the vacuum of fermionic partons ($f_{j,\sigma}|0\rangle = 0\ \forall j,\sigma$) and $d_m^\dagger$ are Bogoliubov–de Gennes (BdG) quasiparticle operators taking the form $d_m^\dagger = \sum_{j=1}^{N}\sum_{\sigma=\uparrow,\downarrow}(U_{m,j\sigma}f_{j,\sigma}^\dagger + V_{m,j\sigma}f_{j,\sigma})$ and satisfying $d_m^\dagger|\Psi_0\rangle = 0$ [26]. This form of $|\Psi_0\rangle$ is particularly suitable for utilizing the MPO-MPS method [18], whose basic idea is summarized as follows [see Fig. 1(b)]: (1) View each $d_m^\dagger$ as an MPO and $|\Psi_0\rangle$ as a tensor network with $2N$ MPOs acting on a product state (parton vacuum); (2) apply these MPOs successively (with a proper order) and compress the outcome in each intermediate step as an MPS with bond dimension up to $\tilde{D}$, which yields an MPS approximating $|\Psi_0\rangle$; (3) apply the Gutzwiller projector P_G to obtain $|\Psi_{\text{MPS}}(\tilde{D})\rangle$, which is an MPS approximation of $|\Psi_G\rangle$. See the Supplemental Material [26] for further technical details.

At each intermediate step of the above MPO-MPS procedure, approximating the MPO-evolved MPS (with bond dimension $2\tilde{D}$) into an MPS (with bond dimension $\tilde{D}$) incurs a truncation error. In order to estimate the accuracy of the final MPS, the accumulated truncation error is defined by

$$\epsilon_{\text{trunc}}(\tilde{D}) = 1 - \prod_{m=1}^{2N} F^{(m)}(\tilde{D}), \quad F^{(m)}(\tilde{D}) = 1 - \sum_{j=1}^{2N} \epsilon_j^{(m)}(\tilde{D}), \tag{5}$$

where $\epsilon_j^{(m)}(\tilde{D})$ is the sum of the discarded squared singular values at the jth bond of the mth MPO-evolved MPS [5]. Notice that $F^{(m)}(\tilde{D})$ is a rough estimate of the overlap between MPO-evolved MPS and truncated MPS in the mth MPO-MPS step.

Since the Hamiltonian $\mathcal{H}_3$ in Eq. (1) is exactly solvable, we also quantify the errors, in both $\Phi_y = \pm 1$ sectors, by comparing the variational energy of the MPS $|\Psi_{\text{MPS}}(\Phi_y, \tilde{D})\rangle$ with the exact ground-state energy $E_g(\Phi_y)$ via the relative energy deviation,

$$\delta E_g(\Phi_y, \tilde{D}) = \frac{\langle\Psi_{\text{MPS}}(\Phi_y, \tilde{D})|\mathcal{H}_3|\Psi_{\text{MPS}}(\Phi_y, \tilde{D})\rangle - E_g(\Phi_y)}{|E_g(\Phi_y)|}. \tag{6}$$

To examine the accuracy of the MPO-MPS method, we compute the truncation error ϵ_{trunc} and the energy deviation δE_g for Hamiltonian $\mathcal{H}_3$ on a cylinder with $L_x \times L_y = 10 \times 4$ and in the sector $\Phi_y = -1$. We take $J_y = J_z = 1$ and vary J_x and J_3 to study both gapped and gapless phases. The results are summarized in Table I. For all these states, as increasing $\tilde{D}$, the truncation errors ϵ_{trunc} are significantly reduced. Nevertheless, the truncation error for the gapless case ($J_x = 1$ and $J_3 = 0$) is clearly larger than those in the gapped phase. It is worth mentioning that, for the case with Abelian topological order ($J_x = 4$ and $J_3 = 0$), the MPO-MPS procedure yields a highly accurate MPS approximation for the ground state. These results give a hint that good MPS approximations of Gutzwiller projected states could be obtained as long as the entanglement has been treated properly.

TABLE I. The truncation error ϵ_{trunc} and the energy deviation δE_g in the MPO-MPS process [see Eqs. (5) and (6)]. The MPO-MPS procedure is carried out for Hamiltonian $\mathcal{H}_3$ with $J_y = J_z = 1$, defined on a cylinder with $L_x \times L_y = 10 \times 4$ and in the $\Phi_y = -1$ sector.

		$J_x = 1$			$J_x = 4$
	$\tilde{D}$	$J_3 = 0$	$J_3 = 0.1$	$J_3 = 0.2$	$J_3 = 0$
ϵ_{trunc}	200	2.4×10^{-2}	1.0×10^{-2}	5.0×10^{-3}	1.0×10^{-6}
	400	2.5×10^{-3}	5.6×10^{-4}	2.4×10^{-4}	3.4×10^{-7}
	800	1.1×10^{-4}	1.9×10^{-5}	7.4×10^{-6}	3.4×10^{-7}
	1000	3.4×10^{-5}	6.8×10^{-6}	2.9×10^{-6}	3.4×10^{-7}
δE_g	200	1.1×10^{-3}	4.9×10^{-4}	1.8×10^{-4}	6.8×10^{-8}
	400	8.8×10^{-5}	2.4×10^{-5}	9.2×10^{-6}	4.9×10^{-8}
	800	4.4×10^{-6}	9.3×10^{-7}	3.3×10^{-7}	4.9×10^{-8}
	1000	1.6×10^{-6}	3.3×10^{-7}	1.3×10^{-7}	4.9×10^{-8}

We now perform DMRG optimization with MPSs prepared from Gutzwiller projected states. For this we consider Hamiltonian $\mathcal{H}_3$ for the challenging gapless case ($J_x = J_y = J_z = 1$ and $J_3 = 0$) [27]. For this particular model, we use the MPO-MPS method to prepare the MPS approximations of the ground states $|\Psi_{\text{MPS}}(\Phi_y, D)\rangle$ in both $\Phi_y = \pm 1$ sectors. For comparison, we also randomly generate an MPS (with bond dimension $\tilde{D}$) and optimize it with the two-site DMRG until a converged MPS with bond dimension D is obtained.

As illustrated in Fig. 3, the relative energy deviation δE_g is reduced by two orders of magnitude with Gutzwiller projected states $P_G|\Psi_0(\Phi_y = \pm 1)\rangle$ being the initial *Ansatz*.

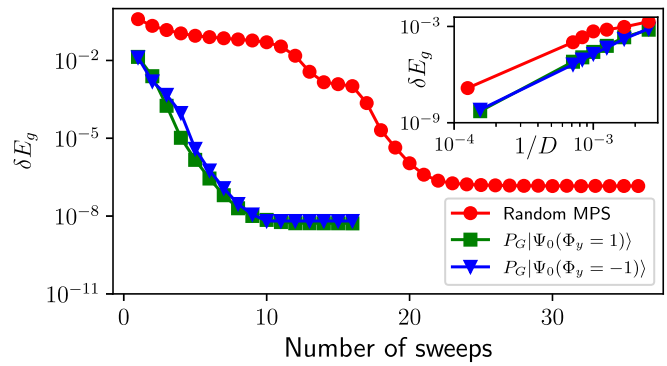

FIG. 3. The relative energy deviations δE_g [Eq. (6)] vs number of sweeps in DMRG. The calculations are performed for the Hamiltonian $\mathcal{H}_3$ in Eq. (1) on an $L_x \times L_y = 6 \times 6$ cylinder and with $J_x = J_y = J_z = 1$ and $J_3 = 0$. The truncation errors are kept to be smaller than 10^{-9} during DMRG optimization. Red, green, and blue lines stand for those with initial states of random MPS, $P_G|\Psi_0(\Phi_y = -1)\rangle$ and $P_G|\Psi_0(\Phi_y = 1)\rangle$, respectively. Note that δE_g initialized with a random MPS is measured from the ground-state energy in the $\Phi_y = -1$ sector. The final bond dimension after DMRG sweeps is $D = 8000$ ($D = 6500$) for random MPS (Gutzwiller *Ansatzë*). Inset: δE_g vs inverse bond dimension $1/D$.

In addition to the substantial improvement of the DMRG results, several remarks are in order: (1) A relatively small bond dimension $\tilde{D} = 200$ for the MPS prepared from $P_G|\Psi_0\rangle$ is sufficiently good to initialize the DMRG process, despite the larger truncation error ($\epsilon_{\text{trunc}} \sim 0.25$) in the MPO-MPS step. Meanwhile, the computational cost of preparing such an MPS with $\tilde{D} = 200$ is quite cheap. (2) During the DMRG sweeps initialized with Gutzwiller projected states, the eigenvalue of the Wilson loop operator ($\Phi_y = \pm 1$) is preserved, i.e., the MPS stays in the respective sector. This is very useful for studying topologically ordered states with topological degeneracy on the cylinder. (3) For the 6×6 cylinder, the DMRG initialized with a random MPS always converges to an MPS in the $\Phi_y = -1$ sector. However, exact results indicate that for a finite cylinder, the ground-state energy in the $\Phi_y = -1$ sector is higher than that in the $\Phi_y = 1$ sector. For instance, the energy difference on the 6×6 cylinder is given by $E_g(\Phi_y = -1) - E_g(\Phi_y = 1) \approx 0.084$. This implies that the DMRG with a random initial *Ansatz* gets stuck in a local minimum [28]. (4) For DMRG initialized with a random MPS, δE_g measured from $E_g(\Phi_y = -1)$ is still about two orders of magnitude larger than those initialized from the Gutzwiller projected state $P_G|\Psi_0(\Phi_y = -1)\rangle$. These clearly show that a properly chosen Gutzwiller projected state provides an ideal initialization *Ansatz* for DMRG in two dimensions.

Diagnosis of parton wave functions. Now we turn to the Kitaev honeycomb model in an external magnetic field along the [111] direction,

$$\mathcal{H} = \sum_{\langle jk\rangle \in a} J_a \sigma_j^a \sigma_k^a - h \sum_j \left(\sigma_j^x + \sigma_j^y + \sigma_j^z\right), \tag{7}$$

with $J_x = J_y = J_z = 1$. With this model, we shall focus on another function of our method, namely, diagnosing whether a Gutzwiller projected state captures the essential entanglement features of the actual ground state for a given Hamiltonian.

In order to diagnose the quality of a Gutzwiller projected parton wave function $P_G|\Psi_{\text{Parton}}\rangle$, we utilize the fidelity defined by [29]

$$F = \text{Tr}\left[\sqrt{\rho_{\text{D}}^{1/2} \rho_{\text{G}} \rho_{\text{D}}^{1/2}}\right], \tag{8}$$

where ρ_{G} and ρ_{D}, being two reduced density matrices for a column of $2L_y$ sites in the middle of the cylinder, correspond to the Gutzwiller *Ansatz* $P_G|\Psi_{\text{Parton}}\rangle$ and the variational ground state $|\Psi_{\text{DMRG}}\rangle$ obtained by DMRG, respectively. This fidelity measures how close are the bulk parts of two wave functions, while the boundary effects are precluded as much as possible. For comparison, we also evaluate the wave-function fidelity $\tilde{F} = |\langle\Psi_{\text{DMRG}}|P_G|\Psi_{\text{Parton}}\rangle|$.

While several parton constructions have been suggested for the Hamiltonian in Eq. (7) (see, e.g., Refs. [20,24,25]), we shall restrict ourselves to four classes of Gutzwiller *Ansatzë*: (1) Kitaev's non-Abelian state with Chern number $C = 1$; (2) fully polarized state with Chern number $C = 0$; (3) partially polarized state with Chern number $C = 1$; and (4) $U(1)$ spin liquid state with a spinon Fermi surface [24]. See the Supplemental Material [26] for further details of these states. The fidelities F and $\tilde{F}$ between these Gutzwiller ansatzes and the variational ground states obtained by DMRG (initialized with random MPSs) are shown in Fig. 4. It is seen that state (1) agrees well with the DMRG-obtained ground state at small h ($0 < h < 0.35$), while both states (2) and (3) coincide with the ground state at large h ($h > 1.25$). For the whole region of h, the $U(1)$ spin liquid state (4) has negligible wave-function fidelity $\tilde{F}$, although the corresponding reduced-density-matrix fidelity F is finite. It is worth noting that the two Gutzwiller projected states (2) and (3) have a large overlap with each other, although their corresponding (unprojected) parton states carry different Chern numbers. For an intermediate magnetic field h ($0.35 < h < 1$), we have observed that the DMRG *cannot* be boosted by any of the four *Ansatzë*, which implies that none of them describes actual ground states well.

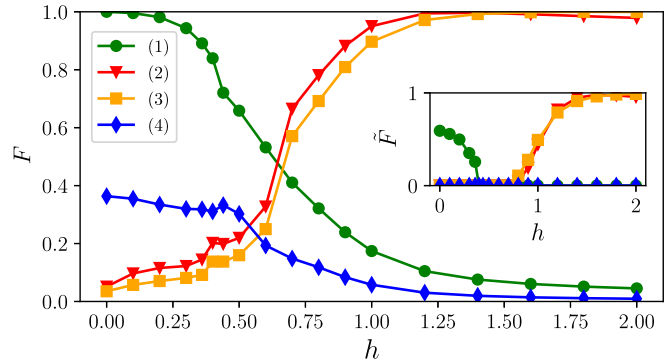

FIG. 4. The fidelities F as a function of the magnetic field h for (1) the Kitaev's non-Abelian state (green), (2) fully polarized state (red), (3) partially polarized state (light blue), and (4) a $U(1)$ spin liquid state (dark blue) [26]. The DMRG calculations generate MPS with bond dimension $D = 2400$ and truncation error $\epsilon_{\text{DMRG}} \sim 10^{-8}$ ($\epsilon_{\text{DMRG}} \sim 10^{-5}$ for $0.4 \leqslant h < 0.7$). Inset: The wave-function fidelity $\tilde{F} = |\langle\Psi_{\text{DMRG}}|P_G|\Psi_{\text{Parton}}\rangle|$.

Discussion. We have devised a method to boost the performance of DMRG in two dimensions by using Gutzwiller projected states as the initialization *Ansatz*. With the extensive benchmarks, our method has shown clear advantages that with a suitably chosen Gutzwiller *Ansatz*, local minima are circumvented and much more accurate results are obtained with no extra computational costs. For topological states, DMRG initialized with a Gutzwiller *Ansatz* can preserve topological sectors, which is very useful for characterizing topological orders [30–33]. Our method also provides a diagnosis tool for analyzing the quality of the Gutzwiller *Ansatz* for a given Hamiltonian. Actually, a number of important strongly correlated systems have elusive ground states, albeit numerous parton wave functions were proposed (see, e.g., Refs. [34–40]). It would be interesting to revisit these problems armed with our method.

Note added. Recently, we became aware of related works [41,42] reporting results on converting Gutzwiller projected wave functions into MPSs and/or using them to initialize DMRG calculations.

Acknowledgments. We thank Qiang-Hua Wang, Yang Qi, Hong Yao, Ying-Hai Wu, Urban Seifert, Yuan Wan, and Zheng Zhu for helpful discussions. This work is supported in part by National Natural Science Foundation of China

(No. 11774306), National Key Research and Development Program of China (No. 2016YFA0300202), the Strategic Priority Research Program of Chinese Academy of Sciences (No. XDB28000000), and the Deutsche Forschungsgemeinschaft (DFG) through project A06 of SFB 1143 (Project No. 247310070).

[1] S. R. White, Phys. Rev. Lett. **69**, 2863 (1992).
[2] S. R. White, Phys. Rev. B **48**, 10345 (1993).
[3] U. Schollwöck, Rev. Mod. Phys. **77**, 259 (2005).
[4] K. A. Hallberg, Adv. Phys. **55**, 477 (2006).
[5] U. Schollwöck, Ann. Phys. **326**, 96 (2011).
[6] S. Östlund and S. Rommer, Phys. Rev. Lett. **75**, 3537 (1995).
[7] J. Dukelsky, M. A. Martín-Delgado, T. Nishino, and G. Sierra, Europhys. Lett. **43**, 457 (1998).
[8] F. Verstraete and J. I. Cirac, Phys. Rev. B **73**, 094423 (2006).
[9] M. B. Hastings, J. Stat. Mech. (2007) P08024.
[10] E. Stoudenmire and S. R. White, Annu. Rev. Condens. Matter Phys. **3**, 111 (2012).
[11] G. Vidal, J. I. Latorre, E. Rico, and A. Kitaev, Phys. Rev. Lett. **90**, 227902 (2003).
[12] J. I. Latorre, E. Rico, and G. Vidal, Quantum Inf. Comput. **4**, 48 (2004).
[13] J. Eisert, M. Cramer, and M. B. Plenio, Rev. Mod. Phys. **82**, 277 (2010).
[14] C. Gros, Ann. Phys. (NY) **189**, 53 (1989).
[15] P. W. Anderson, P. A. Lee, M. Randeria, T. M. Rice, N. Trivedi, and F. C. Zhang, J. Phys.: Condens. Matter **16**, R755 (2004).
[16] P. A. Lee, N. Nagaosa, and X.-G. Wen, Rev. Mod. Phys. **78**, 17 (2006).
[17] Y. Zhou, K. Kanoda, and T.-K. Ng, Rev. Mod. Phys. **89**, 025003 (2017).
[18] H.-K. Jin, H.-H. Tu, and Y. Zhou, Phys. Rev. B **101**, 165135 (2020).
[19] Y.-H. Wu, L. Wang, and H.-H. Tu, Phys. Rev. Lett. **124**, 246401 (2020).
[20] A. Kitaev, Ann. Phys. **321**, 2 (2006).
[21] Z. Zhu, I. Kimchi, D. N. Sheng, and L. Fu, Phys. Rev. B **97**, 241110(R) (2018).
[22] M. Gohlke, R. Moessner, and F. Pollmann, Phys. Rev. B **98**, 014418 (2018).
[23] C. Hickey and S. Trebst, Nat. Commun. **10**, 530 (2019).
[24] H.-C. Jiang, C.-Y. Wang, B. Huang, and Y.-M. Lu, arXiv:1809.08247.
[25] M.-H. Jiang, S. Liang, W. Chen, Y. Qi, J.-X. Li, and Q.-H. Wang, Phys. Rev. Lett. **125**, 177203 (2020).
[26] See Supplemental Material at http://link.aps.org/supplemental/10.1103/PhysRevB.104.L020409 for more details, which includes Refs. [43–48].
[27] The loop-gas state introduced in Ref. [49] would be a nice initialization *Ansatz* for DMRG. However, its MPS representation has a bond dimension $D = 7^{L_y}$, which, for $L_y = 6$, is beyond the capacity of DMRG.
[28] We have performed DMRG sweeps with an unbiased set of random MPS up to 36 times. Starting from the 24th sweep, the variational energy no longer decreases and becomes fluctuating, and the relative energy deviation δE_g in the 36th sweep is almost identical to the one in the 24th sweep (the difference is about 10^{-8}), indicating that the randomly initialized DMRG gets stuck in a local minimum.
[29] I. McCulloch, arXiv:0804.2509.
[30] Y. Zhang, T. Grover, A. Turner, M. Oshikawa, and A. Vishwanath, Phys. Rev. B **85**, 235151 (2012).
[31] L. Cincio and G. Vidal, Phys. Rev. Lett. **110**, 067208 (2013).
[32] H.-H. Tu, Y. Zhang, and X.-L. Qi, Phys. Rev. B **88**, 195412 (2013).
[33] M. P. Zaletel, R. S. K. Mong, and F. Pollmann, Phys. Rev. Lett. **110**, 236801 (2013).
[34] S. Yan, D. A. Huse, and S. R. White, Science **332**, 1173 (2011).
[35] S. Depenbrock, I. P. McCulloch, and U. Schollwöck, Phys. Rev. Lett. **109**, 067201 (2012).
[36] H. J. Liao, Z. Y. Xie, J. Chen, Z. Y. Liu, H. D. Xie, R. Z. Huang, B. Normand, and T. Xiang, Phys. Rev. Lett. **118**, 137202 (2017).
[37] Y.-C. He, M. P. Zaletel, M. Oshikawa, and F. Pollmann, Phys. Rev. X **7**, 031020 (2017).
[38] Y. Ran, M. Hermele, P. A. Lee, and X.-G. Wen, Phys. Rev. Lett. **98**, 117205 (2007).
[39] Y. Iqbal, F. Becca, S. Sorella, and D. Poilblanc, Phys. Rev. B **87**, 060405(R) (2013).
[40] T. Li, arXiv:1807.09463.
[41] G. Petrica, B.-X. Zheng, G. K.-L. Chan, and B. K. Clark, Phys. Rev. B **103**, 125161 (2021).
[42] A. M. Aghaei, B. Bauer, K. Shtengel, and R. V. Mishmash, arXiv:2009.12435.
[43] A. A. Abrikosov, Phys. Phys. Fiz. **2**, 61 (1965).
[44] F. J. Burnell and C. Nayak, Phys. Rev. B **84**, 125125 (2011).
[45] Y.-Z. You, I. Kimchi, and A. Vishwanath, Phys. Rev. B **86**, 085145 (2012).
[46] X.-G. Wen, Phys. Lett. A **300**, 175 (2002).
[47] X.-G. Wen, Phys. Rev. B **65**, 165113 (2002).
[48] Y. Zhou and X.-G. Wen, arXiv:cond-mat/0210662.
[49] H.-Y. Lee, R. Kaneko, T. Okubo, and N. Kawashima, Phys. Rev. Lett. **123**, 087203 (2019).